Ion-Induced Stabilization of the G-DNA Quadruplex: Free Energy Perturbation Studies

Wilson S. Ross† and Charles C. Hardin*,‡

Contribution from the Department of Pharmaceutical Chemistry, University of California, San Francisco, California 94143, and Department of Biochemistry, North Carolina State University, Raleigh, North Carolina 27695

Received May 17, 1993. Revised Manuscript Received March 28, 1994•

Abstract: Free energy perturbation calculations were used to determine how the size of an internally bound monovalent cation affects the stability of an antiparallel G-DNA quadruplex in water. A free energy cost was incurred as the cation size was increased in both water and within the DNA 'host' complex. In water the free energy tends to level off as the ionic radius increases and charge density correspondingly decreases. In contrast, in the DNA complex the free energy change became progressively steeper as the growing ion began to induce conformational deformations in the relatively constrained binding site. The minimum point in the energy curve obtained by subtracting the free energy curves for water and DNA indicates the favored cation for binding within the complex. Two sets of ionic Lennard-Jones '6–12' van der Waals parameters were tested and gave similar results. In both cases the minimum free energy is in the middle of the size range of the monovalent monoatomic cations, in qualitative agreement with experimental results. However, K^+ is apparently too big for the DNA cavity, leading to weakening of the solvent-exposed, outer hydrogen bonds, so that Na^+ is wrongly preferred. Thus, in contrast to expectation, the steric fit of group IA cations may not be the sole determinant of ion selectivity; *e.g.*, K^+-specific electronic effects may be involved. An antiparallel closed-loop model for the DNA sequence $d(T_2G_4)_4$ was also constructed by adding two covalently-connected thymidine residues to close each major groove at one end of the quadruplex stem and each minor groove at the other end. Interloop thymidine–thymidine base pairing interactions formed at each end during molecular dynamics trajectories that were started from several different initial loop configurations.

Experimental studies have shown that monoatomic cations can induce radical changes in structures that are adopted by guanine-rich DNAs.[2-10] For example, stabilization of the quadruplex structure formed by four strands of d(CGC G_3 GCG) depends on the radius and charge of internally bound cations.[3] Structural studies with several molecules showed that both the stability and strand polarity of quadruplexes are affected by DNA sequence.[3,4,9,10] Monovalent cations stabilize the parallel-stranded quadruplex formed by d(CGC G_3 GCG) in the order $K^+ > Na^+ > Li^+$ (by decreasing size) and $K^+ > Rb^+ > Cs^+$ (by increasing size) while the order for the divalent cations is ($K^+ >$) $Ca^{2+} > Mg^{2+}$ (by decreasing size). A similar order of monovalent cation-dependent stabilities was also obtained with quadruplex structures formed by the *Tetrahymena*, human, and *Dictyostelium* telomeric DNA sequences $d(T_2G_4)_4$, $d(T_2AG_3)_4$, and $d(AG_6\ GAG\ AG_6\ AG_6)$.[4]

Descriptions of the stabilizing effects of cations on nucleic acid structures have traditionally addressed the more common mechanism of 'counterion condensation',[11] in which stabilization is due to electroneutralization of anionic phosphodiester groups by cations and the consequent decrease in macromolecular linear charge density. These effects involve long-range electrostatic interactions between the polyanionic phosphodiester backbone and the condensed counterions. The case considered here is distinctly different.[8] A structural explanation has been proposed for the large differences in the stabilities of complexes formed by specific cations and G-rich DNAs.[4,12] These complexes consist of eight guanines which condense to form two stacked planar 'G-quartet' base assemblies, thus trapping the cation within a cavity that is lined by eight hydrogen-bonded carbonyl oxygen atoms (GO6[1]) in a nearly octahedral geometry (Figure 1). Assuming that the optimum interatomic distances are similar to those found in the X-ray crystal structures of [crown ether·cation] complexes, potassium fits snugly within the cavity in the center of the quadruplex.[8,12] In contrast, the other ions may disrupt the DNA structure more than that of water, the smaller ions perhaps by drawing the oppositely-charged GO6 atoms into a partially vacant central cavity and the larger ones by steric disruption of the hydrogen bonds between the strands. The differential stabilizing effect of cations has been proposed as the driving force for an ion-dependent switching mechanism that may control transitions between different DNA structures and thus regulate genetic functions.[3-7]

The [quadruplex·$cation_n$] structure is comparable to those of host–guest (or cryptand) complexes formed by crown ether molecules and monoatomic cations.[13] However, the *poly-ether* ligands have the flexibility to wrap around a fairly broad range of cation sizes without becoming highly destabilized. In contrast, interstrand hydrogen bonds between the guanine (*imide*) carbonyl ligands and imino hydrogens must be strained or disrupted to accommodate larger ions within the highly confined central spine of the quadruplex. A third type of host–guest complex is formed

† University of California, San Francisco.
‡ North Carolina State University.
• Abstract published in *Advance ACS Abstracts*, June 1, 1994.

(1) Abbreviations: FEP-MD, free energy perturbation/molecular dynamics; O_{GO6}, guanine O6 oxygen atom; O_{H_2O}, water oxygen atom; Pu, purine; Py, pyrimidine.

(2) Henderson, E.; Hardin, C. C.; Wolk, S. K.; Tinoco, I., Jr.; Blackburn, E. H. *Cell* **1987**, *51*, 887–908.
(3) Hardin, C. C.; Watson, T.; Corregan, M.; Bailey, C. *Biochemistry* **1992**, *31*, 833–841.
(4) Hardin, C. C.; Henderson, E.; Watson, T.; Prosser, J. K. *Biochemistry* **1991**, *30*, 4460–4472.
(5) Sen, D.; Gilbert, W. *Nature* **1988**, *334*, 364–366.
(6) Sen, D.; Gilbert, W. *Nature* **1990**, *344*, 410–414.
(7) Williamson, J. R.; Raguhuraman, M. K.; Cech, T. R. *Cell* **1990**, *59*, 871–880.
(8) Guschlbauer, W.; Chantot, J.-F.; Thiele, D. *J. Biomol. Struct.*, **1990**, *3*, 491–511.
(9) Jin, R.; Breslauer, K. J.; Jones, R. A.; Gaffney, B. L. *Science* **1990**, *250*, 543–546.
(10) Wang, Y.; de los Santos, C. D.; Gao, X.; Gaffney, B. L.; Jones, R.; Breslauer, K. J.; Live, D. L.; Patel, D. *Biophys. J.* **1991**, *59*, 439a.
(11) Record, M. T., Jr.; Anderson, C. F.; Lohman, T. M. *Q. Rev. Biophys.* **1978**, *2*, 103–178.
(12) Sundquist, W. I.; Klug, A. *Nature* **1989**, *342*, 825–829.
(13) Grootenhuis, P. D. J.; Kollman, P. A. *J. Am. Chem. Soc.* **1989**, *111*, 2152–2158.

0002-7863/94/1516-6070$04.50/0 © 1994 American Chemical Society

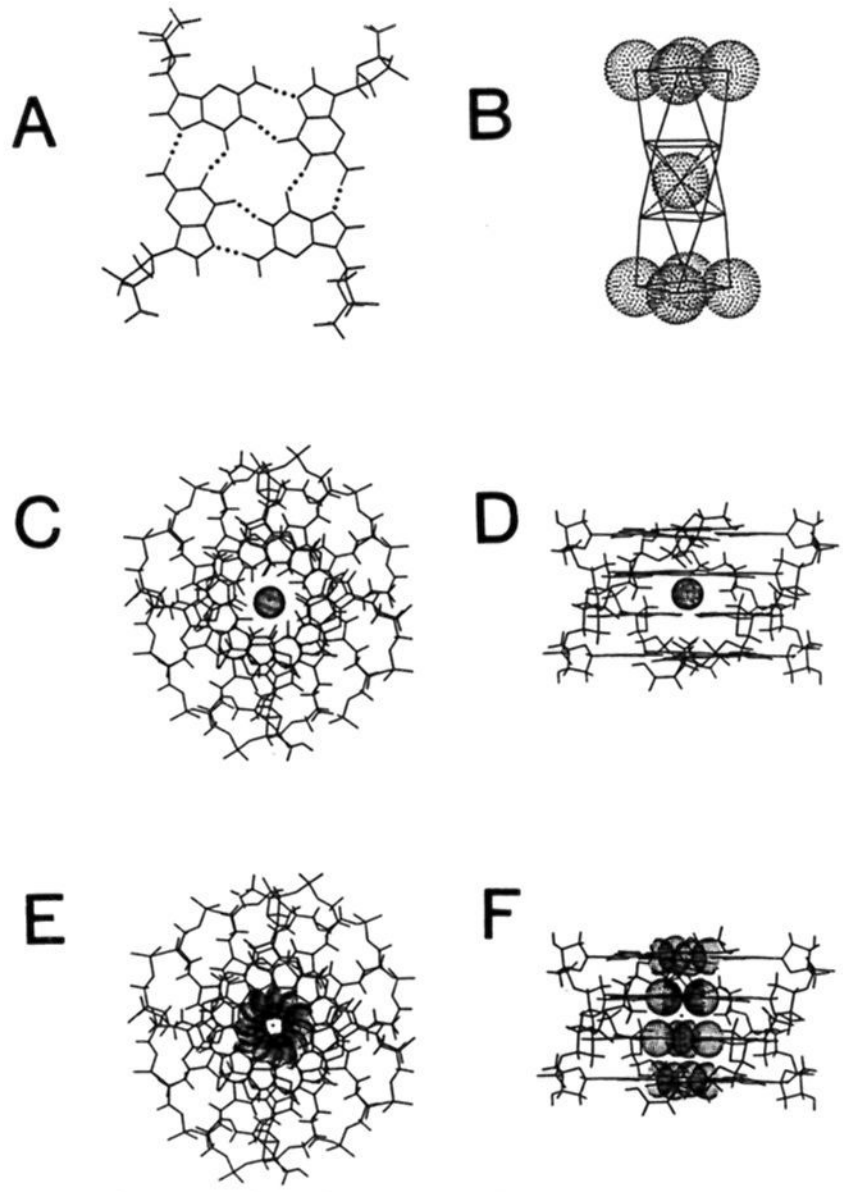

Figure 1. Structure of the 'G-quartet' and G-DNA quadruplex structural motifs. (A) The 'G-quartet'. Strand polarities are antiparallel; *syn* and *anti* glycosidic torsion angles are shown, as expected for the antiparallel structure.[2,8,39] (B) 'Twisted cage' formed by the GO6 atoms. The van der Waals radii of the bound ion (in the center) and terminal GO6 atoms are shown. (C) Axial view of a quadruplex with a 'guest' cation between the two central 'G-quartets'. (*D*) Side view of the quadruplex with a guest cation, major groove facing viewer. (E) Axial view of the central 'tube' formed by GO6 atoms. (F) Side view of the central GO6 tube.

between the peptide ionophore valinomycin and monovalent cations, representing an intermediate situation in terms of ion constraint.[14] In that case, *amide* carbonyl ligands participate both in ion binding and in stabilization of the bracelet-like conformation of the host via intramolecular hydrogen bonding to the amide hydrogens.

Grootenhuis and Kollman[13] used free energy perturbation/molecular dynamics (FEP-MD) calculations to assess the relative stabilities of [dibenzo-30-crown-10–cation] complexes in water. These calculations involved converting (perturbing) the ionic radius from that of Li^+ to that of Cs^+ and calculating free energy values at discrete steps along the 'reaction' pathway using coordinates obtained from molecular dynamics trajectories. Free energies obtained for ion-induced stabilization of the [dibenzo-30-crown-10–cation] complex were on the order of 1 kcal per mol of bound ion.[13] Eisenman *et al.*[14] used *in vacuo* FEP-MD calculations to determine the ion selectivity of valinomycin with refined amide carbonyl partial charges and Lennard-Jones 6–12 parameters. The ion-selectivity pattern was found to be strongly dependent upon the magnitude of the partial charge used for the carbonyl oxygen.

In this study, FEP-MD calculations were used to determine the relative stabilities of quadruplex–monocation 'host–guest' complexes as a function of cation size. It was found that steric fit of the ion in the cavity does not appear to fully explain selectivity of K^+ over Na^+, although otherwise reasonable agreement was obtained between the calculated results and experimentally determined trends in the stabilities of [DNA quadruplex·Group IA cation] complexes.

(14) Eisenman , G.; Åqvist, J.; Alvarez, O. *J. Chem Soc., Faraday Trans.* **1991**, *87*, 2099–2109.

Experimental Section

The AMBER 'all-atom' force field for DNA[15] and the TIP3 water force field[16] were used for all simulations in combination with various ion parameters described below. The AMBER 3.0 Revision A,[17] 4.0,[18] and 4.1 programs were used for the calculations. The CARNAL program, a new addition to AMBER, was used for trajectory analysis. The UCSF MIDASPlus graphics program[19] was used for solute model building.

Each dynamics trajectory was prepared by gradually warming the system to 300 K and then allowing it to equilibrate. In some cases, a central cation was then perturbed from one type of monovalent cation to another by changing the van der Waals parameters. van der Waals interactions are parametrized by Lennard-Jones (L-J) 6–12 potentials of the form

$$E_{vdw} = \frac{A_i A_j}{r_{ij}^6} - \frac{B_i B_j}{r_{ij}^{12}}$$

where A and B parameters for atoms of types i and j are derived to fit a given potential between two atoms of the same type. This same-type potential curve can also be parametrized by the *radius* (r^*) corresponding to half the internuclear distance at the point of minimum energy, and the *potential well depth* (e) at that internuclear distance. In this convention, the potential energy for the van der Waals interaction between atoms i and j is defined as (r_{ij}^*, e_{ij}), where $r_{ij}^* = (r_i^* + r_j^*)$, and $e_{ij} = -e_i e_j$. This is the convention which is used by AMBER. Note that the different "combining rules" for the (A, B) and (r^*, e) conventions are equivalent for pairs of atoms of the same type but result in different potentials when applied to a given pair of atoms of different types.

In the first set of free energy calculations, the ionic charge was perturbed to study absolute hydration and complexation energies of Li^+. In the second set of calculations, L-J parameters were perturbed to vary the cation size in order to determine relative hydration and complexation free energies. Two protocols were used for the L-J perturbations: in the first, only the ion r^* value was changed, while holding the well depth constant. Ion/O_{H_2O} and ion/O_{GO6} radial distribution function first peaks were used to relate r^* parameters to the actual internuclear distances. In the second L-J prootocol, both r^* and e were perturbed simultaneously using L-J parameters adapted from Åqvist.[20] The 'windows' method was used for the perturbation calculations. For each value i of the dimensionless window parameter λ, the system was equilibrated and then ΔG values corresponding to $\lambda_i \pm \Delta\lambda$ were calculated over an ensemble of the ensuing states (coordinate sets).[21]

A mass of 6.94 au (corresponding to Li^+) was used for the perturbed ion to increase the sampling efficiency. The use of constant mass in free energy perturbations is a standard practice[22] because the equilibrium properties of a system (as opposed to its transport or relaxation properties) are not dependent on the kinetic part of the Hamiltonian (*i.e.* average relative velocities are 0)[23] and because mass contributions are expected to cancel across any thermodynamic cycle.[13,24] This point is examined further below.

DNA strands were terminated by hydrogen atoms. For solvated DNA, Na^+ counterions (charge = $1e^+$, $r^* = 1.2$ Å , $e = 0.1$ kcal mol^{-1}) were placed 4.5 Å from the backbone phosphate groups on the O–P–O bisector.

(15) Weiner, S. J.; Kollman, P. A.; Case, D. A.; Singh, U. C.; Ghio, C.; Alagona, G.; Profeta, S., Jr.; Weiner, P. *J. Am. Chem. Soc.* **1984**, *106*, 765–783.

(16) Jorgensen, W. L. ; Chandrasekhar, J.; Madura, J. D.; Impey, R. W.; Klein, M. L. *J. Chem. Phys.* **1983**, *79*, 926–935.

(17) Seibel, G. (revision author); Singh, U. C.; Weiner, P. K.; Caldwell, J.; Kollman, P. A. *AMBER 3.0 Revision A*; University of California, San Francisco, 1989.

(18) Pearlman, D. A.; Case, D. A.; Caldwell, J. C.; Seibel, G. L.; Singh, U. C.;Weiner, P. K.; Kollman, P. A. *AMBER 4.0*; University of California, San Francisco, 1991. Pearlman, D. A., Free energy program (Gibbs).

(19) Huang, C.; Pettersen, E.; Ferrin, T.; Langridge, R. *MidasPlus*; University of California, San Francisco, 1989. Ferrin, T. E.; Wang, C. C.; Jarvis, L. E.; Langridge, R. J. *Mol. Graphics* **1988**, *6*, B-27.

(20) Åqvist, J. *J. Phys. Chem.* **1990**, *94*, 8021–8024.

(21) Singh, U. C.; Brown, F. K.; Bash, P. A.; Kollman, P. A. *J. Am. Chem. Soc.* **1987**,*109*, 1607–1614.

(22) van Gunsteren, W. F.; Mark, A. E. *Eur. J. Biochem.* **1992**, *204*, 947–961.

Counterions were treated as part of the solute for calculations of nonbonded interactions. All solvated systems were in the NPT ensemble, at a pressure of 1 atm and temperature of 300 K. Water molecules were placed by AMBER to provide a given clearance between the solute atom centers (including counterions for DNA) and the nearest side of the initial periodic box. A cutoff distance of 8 Å was used for nonbonded interactions, except when evaluating solute–solute interactions, where no cutoff was applied in order to maintain DNA charge neutralization by counterions. Since the counterions remain within 8 Å of the DNA, the 8-Å water–water and solute–water cutoff is sufficient for the local interactions in the vicinity of the backbones, *i.e.* between phosphate groups, water, and counterions. Time steps of 0.002 ps were used in all of the dynamics calculations. The SHAKE algorithm[25] was used to constrain covalent bonds involving hydrogens.

Results and Discussion

Quadruplex Model-Building Studies. Williamson *et al.*[7] proposed a structure for the four-stranded complex $d(G_4)_4$, in which the adjacent strands are antiparallel and alternate strands have uniform *syn* or *anti* glycosidic torsion angles, with alternating major and minor grooves around the long axis. The structure was based on X-ray fiber diffraction results obtained with poly-[r(I)],[26] which has a right-handed axial twist of 30° and several conformational features that resemble those of canonical A-form structures.[7,27] For the present study, the Williamson model was optimized by constraining the bases in place while allowing the backbone to move during *in vacuo* molecular dynamics at 10 K. The structure was then equilibrated with counterions in a water bath, a part of the trajectory was root mean square fit to the central 8 GO6 atoms of a reasonable-looking structure, and the coordinate sets were averaged over the trajectory and then energy minimized *in vacuo*. The energies of the initial and final structures were 9.2×10^9 and -7.4×10^2 kcal mol^{-1}, respectively, although the overall structure remained quite similar. During *in vacuo* dynamics with the bases constrained, the phosphodiester backbone undulated in a motion that involved rotation about the glycosidic bond of the fixed 5′-terminal base. As a result, the 5′ ends periodically 'dove' in toward the adjacent minor grooves, apparently attracted by the phosphate negative charge density. When the constraints were removed, this diving motion pulled the attached bases, distorting the stacking and hydrogen bonding between the residues at the ends.

In order to avoid end effects, we made an effort to provide a plausible, yet minimal, end environment using the *Tetrahymena* telomere sequence $d(TTGGGG)_n$. A single-stranded closed-loop G-DNA complex was built by adding loops consisting of two thymidines to covalently link the ends of the relaxed four-stranded model, still holding the Gs fixed and letting the backbone and Ts relax during 10 K dynamics. The Ts relaxed to similar stacked positions starting from several different hand-built structures (Figure 2). While this structure is not expected to occur in a chromosome because it is a small closed loop, it provides two different types of end environment to study, either of which might occur in a chromosome or chromosome–chromosome complex.[4,6,7] The covalent TT loops closed the minor grooves on one end of the quadruplex stem and the major grooves on the other. The end with the closed minor groove and open major groove dissociated more readily when the unconstrained model was subjected to 300 K dynamics *in vacuo* with monovalent counterions placed near the backbone phosphates.

At 300 K with 2415 waters and counterions, the hydrated four-stranded structure was not disrupted by the attraction of the 5′-terminal sugars for the minor groove that was observed *in vacuo*. Instead, after about 20 ps the 3′-terminal sugars at one end began to extend into solution while the central parts of the attached bases remained in place. By *ca.* 40 ps the two bases formed a 'V' that pointed toward the center of the adjoining plane with each base inclined at an *ca.* 45° angle relative to the planar surfaces of the other bases. The strand neighbors of these two bases (in the second, adjacent plane) moved diagonally toward each other and closer to the helix axis, while the other two bases in the adjacent plane moved away from the axis. The bases in the third plane remained quite close to their original conformation. This produced a worsening of the best root mean square fit positions of the bases in the central two planes from 0.6 to 1.0 Å. However, at least one hydrogen bond was maintained in each of the four terminal base pairs at the disrupted end, and the bases in the two central G-quartets remained stacked. This structure was stable until the end of the run (an additional 44 ps). Displacement of the 3′-terminal bases (rather than the 5′-terminal ones in the adjacent strands) might occur because the 3′-terminal deoxyriboses 'overhang' the major grooves to a greater extent (Figure 1D, upper foreground) and are thus more exposed to solvent. The change might occur only at one end due to the asymmetry of the structure, which has two diagonally opposite parallel strands with *syn* glycosidic torsion angles, with the other two strands running in the opposite direction and containing *anti* nucleosides.

The closed-loop $d(T_2G_4)_4$ model was also supplied with counterions and hydrated, and then the system was warmed to 300 K. Stacking and hydrogen bonding remained stable for a 4-ps run. The final structure is shown in Figure 2. Constraining the ends by adding the loops resulted in widening of the minor grooves and narrowing of the major grooves, producing a more symmetric overall structure. Also, *interloop* base-pairing interactions between the thymidine residues in each covalent loop and stacking interactions between the thymidines and the adjacent guanines may have helped to stabilize the terminal 'G-quartets' in the quadruplex stem.

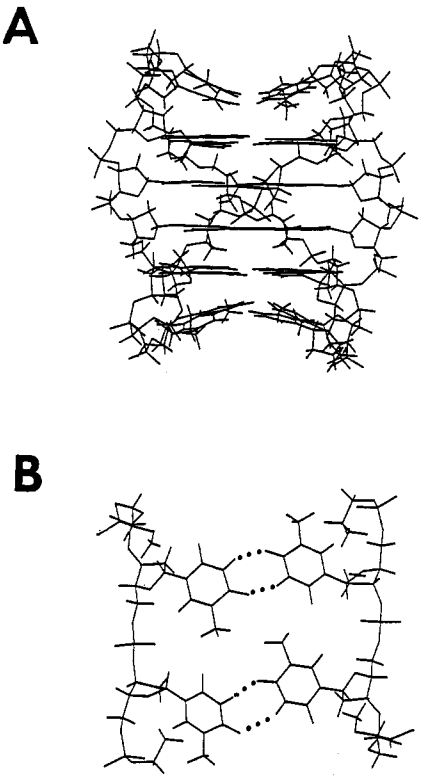

Figure 2. Antiparallel quadruplex formed by the cyclized single-stranded 24-mer $d(T_2G_4)_4$. (A) Side view showing the stacking geometry of the bases. Note how the base-paired thymidine residues are pulled in toward the central axis and the adjacent stacked G-quartets. (B) Intrastrand T·T base pairs formed by the loop residues in the complex.

(23) Bennett, C. H. *J. Comput. Phys.* **1975**, *19*, 267–279.
(24) McQuarrie, D. A. *Statistical Mechanics*; Harper & Row, New York, 1976; pp 416–417, 441.
(25) van Gunsteren, W. F.; Berendsen, H. J. C. *Mol. Phys.* **1977**, *34*, 1311–1327.

Kang *et al.*[28] solved the crystal structure of *Oxytricha* telomeric DNA, $d(G_4T_4G_4)_2$. The bimolecular complex contained adjacent antiparallel strands, alternating *syn/anti* guanine glycosyl conformations in each strand, and alternating major/minor grooves. Smith and Feigon[29] solved the solution structure of the same sequence using NMR. Alternating *syn/anti* glycosidic torsion angles were detected; however the loops of the two strands were entwined in an 'Indian key' structure[30] rather than the (side-by-side) 'Greek key' structure of Kang *et al.* The thymine residues were removed from one of the two molecules in the asymmetric unit of the Kang *et al.* structure, and two folded-in backbone phosphates were reoriented by hand to allow placement of counterions along the O–P–O bisector. Although this model was initially somewhat wrinkled in appearance owing to slight deviations of the bases from coplanarity, during dynamics equilibration the bases immediately assumed a regular, coplanar orientation. As with the Williamson model, the structure with the reoriented phosphates was equilibrated with counterions in a water bath, a part of the trajectory was root mean square fit to the central eight GO6 atoms of a reasonable-looking structure, the resulting coordinate sets were averaged, and this structure was minimized *in vacuo*. The energies of the initial and final structures were 1.0×10^3 and -7.3×10^2 kcal mol^{-1}, respectively.

When the four-stranded Kang *et al.* and the closed-loop Williamson *et al.* structures were provided with a full complement of three complexed ions, the two end ions drifted out of the complex. When the ions were linked by harmonic distance restraints in the Kang model, the DNA structure was disrupted.

Ion L-J Potential Parametrization in H_2O and Quadruplex DNA. Two problems were faced in parametrizing the ions: (i) a lack of experimental data for ionic radii in analogous model complexes and (ii) the different force fields for DNA and water. In the absence of experimental data, it was initially assumed that ion–oxygen radii in the complex are the same as in water. TIP3 water, which was parametrized for water–water interactions, uses a large oxygen van der Waals radius to encompass the entire water molecule. The O_{TIP3} r^* = 1.768 Å and e = 0.152 kcal mol^{-1}, while the AMBER parameters for the carbonyl O_{GO6} are r^* = 1.6 Å and e = 0.2 kcal mol^{-1}. Thus, given the same well depth, ions must have *different* r^* *values* for water and DNA to achieve the same ion–oxygen internuclear distance.

One set of ion van der Waals parameters was derived by choosing a 0.1 kcal mol^{-1} well depth, varying r^*, and determining the ion–oxygen radial distribution functions from multiple molecular dynamics trajectories in water and within the complex. The ion–oxygen internuclear distance at the first peak of each radial distribution curve was plotted as a function of the r^* parameter used to obtain the curve, and then a linear function was fitted to the data for each environment (Figure 3). When the ion size in DNA became large enough to disrupt the quadruplex structure at r_{ion}* values of 3 and 3.5 Å, a cavity was formed in the DNA and the peak of the ion–oxygen radial distribution was located at 4.35 Å for both r_{ion}* values, which did not conform to the linear fit obtained with smaller radii. First-peak internuclear distances obtained from experimental ion–O_{H2O} radial distribution data were substituted into the linear functions to obtain r^* values for different cations in water and within the complex (Table 1).

As discussed below, these simple ion parameters can be used to generate qualitatively correct and structurally interpretable free energy results. Moreover, these parameters yield quantitatively correct relative energies of cation hydration. For example, the free energy calculated for the Li^+ to K^+ perturbation in H_2O (*ca.* 40 kcal mol^{-1}) is about the same as experimentally determined

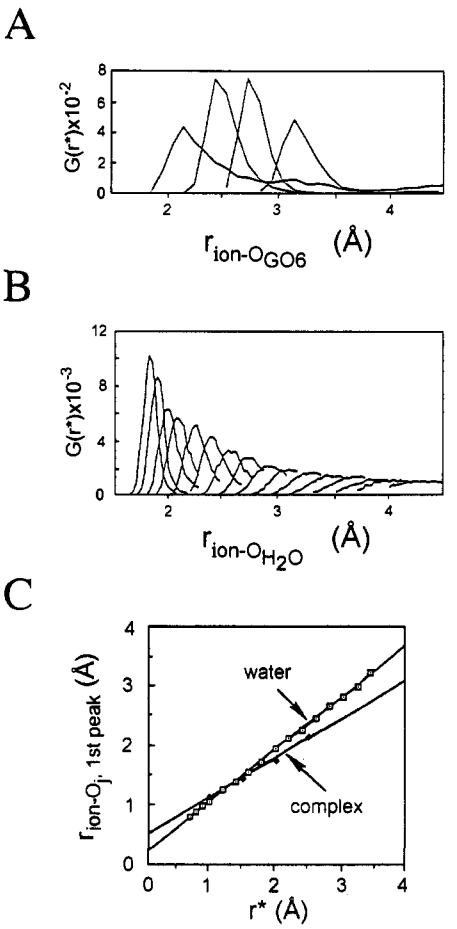

Figure 3. Radial distribution functions $G(r)$ for parametrizing and checking the nonbonded ionic interaction potential functions. Each curve in parts A and B represents the ion–oxygen radial distribution for a given value of r^*. $G(r)$ units reflect the number of sampled distances in the DNA quadruplex and H_2O populations. (A) O_{GO6}–ion radial distribution functions for ion r^* parameters of 1.0, 1.5, 2.0, and 2.5 Å, left to right by first peaks. (B) O_{H_2O}–ion radial distribution functions for ion r^* parameters of 0.7, 0.8, 0.9, 1.0, 1.2, 1.4, 1.6, 1.8, 2.0, 2.2, 2.4, 2.6, 2.8, 3.0, 3.2, and 3.4 Å, left to right by first peaks. (C) Linear fits of the oxygen–ion first peak radii for the water (⊡) and quadruplex (♦) calculations. Equations for the lines are $r(O_{H_2O}\text{–ion}) = 0.88r^*_{ion} + 1.17$ and $r(O_{GO6}\text{–ion}) = 0.66r^*_{ion} + 1.47$.

values of 43[31] and 45 kcal mol^{-1}.[32] This is much closer than the value of 67 kcal mol^{-1} obtained by Migliore *et al.*[33] using parameters that were fitted to potential energies from *ab initio* calculations in FEP calculations using Monte Carlo methods to generate coordinate ensembles. However when Corongiu *et al.*[34] used an *ab initio*-derived potential with 'three-body' interactions in a later study to determine the free energy of hydration for Li^+, a more accurate result was obtained (4% less than the experimental value vs 16% greater than experiment in the study of Migliore *et al.*[33]). The hydration free energy obtained with our simple parameters is −118 kcal mol^{-1}, which compares well to experimental values of −118.1 and −123.5 kcal mol^{-1}, as discussed below.

Heretofore, most ion L-J parametrization has consisted of fitting the molecular mechanics potential to quantum mechanical results for a set of ion–water conformations.[13,33-43] An alternative

(26) Zimmerman, S. B.; Cohen, S. B.; Davies, D. R. *J. Mol. Biol.* **1975**, *92*, 181–192.
(27) Saenger, W. *Principles of Nucleic Acid Structure*; Springer-Verlag: New York, 1984; p 317.
(28) Kang, C.; Zhang, X.; Ratliff, R.; Moyzis, R.; Rich, A. *Nature* **1992**, *356*, 126–164.
(29) Smith, F. W.; Feigon, J. *Nature* **1992**, *356*, 164–168.
(30) Frank-Kamenetskii, M. *Nature* **1992**, *356*, 105.
(31) Friedman, H. L.; Krishnan, C. V. In: *Water: A Comprehensive Treatise*; Franks, F., Ed.; Plenum Press, New York, 1973; Vol. 3.
(32) Gomer, R.; Tryson, G. J. *J. Chem. Phys.* **1977**, *66*, 4413–4424.
(33) Migliore, M.; Corongiu, G.; Clementi, E.; Lie, G. C. *J. Chem. Phys.* **1988**, *88*, 7766–7771.
(34) Corongiu, C.; Migliore, M.; Clementi, E. *J. Chem. Phys.* **1989**, *90*, 4629–4630.
(35) Clementi, E.; Popkie, H. *J. Chem. Phys.* **1972**, *57*, 1077–1094.

Table 1. Lennard-Jones 6–12 Parameters Used for the Ions in This Study

				ion parameter convention				
				e = 0.1		Åqvist/TIP3 (AMBER) ions		
ion	r(cryst)[a] (Å)	r(ion–O_{H_2O}) (Å)	r('target')[f] (Å)	r^*(water)[g] (Å)	r^*(DNA)[h] (Å)	r^*[i] (Å)	e[i] (kcal)	r(ion–O_{GO6}) (Å)
Li^+	0.6	1.95–2.25[b]	2.03	0.97	0.84	1.14	0.018 279	2.05
Na^+	0.95	2.35–2.42[c]	2.39	1.38	1.39	1.87	0.002 772	2.40
K^+	1.33	2.80–3.1[d]	2.75	1.79	1.93	2.66	0.000 328	2.67
Rb^+	1.48	2.88[e]	2.89	1.95	2.14	2.96	0.000 171	2.75
Cs^+	1.69	3.15[e]	3.10	2.20	2.46	3.40	0.000 081	2.95

[a] See ref 47. [b] 1.95 ± 0.02 Å/3.57 mol of LiCl (neutron diffraction), see ref 48; 1.95–2.25 Å (X-ray diffraction), see ref 49. [c] 2.38, 2.4 Å (X-ray diffraction), see ref 49; 2.42 Å, see ref 50. [d] 2.80 Å, see ref 50; 2.9 Å (X-ray diffraction), see ref 51; 3.1 Å (neutron diffraction), see ref 52. [e] See ref 50. [f] Adopted for comparison from ref 20. Note that K^+ is closer to the sum of Pauling radii (2.70 Å) than experimental results for solution (2.80–3.1 Å). [g] From equation of Figure 3: $r(O_{H_2O}\text{–ion}) = 0.88r^*_{ion} + 1.17$ Å. [h] From equation of Figure 3: $r(O_{GO6}\text{–ion}) = 0.66r^*_{ion} + 1.47$ Å. [i] From ref 17, adapted for AMBER[15] combining rules with TIP3 water.[16]

approach is to fit the nonbonded parameters for the ion to experimentally-determined *ensemble* characteristics: ion–O_{H_2O} radial distribution first peaks and free energies. This macroscopic ensemble-averaged dynamics approach has been used by Åqvist[20] to derive L-J parameters for ions in SPC water[44] that achieve correct relative and absolute ion solvation free energies using the SCAAS method[45] to simulate infinite dilution. The same parameters also fit the first peaks and hydration free energies with TIP3 water using periodic boundary conditions, after adjustment for the AMBER combining rules to give the same ion–water r^* [46] (the well depth is not as sensitive as r^* to the combining rules). We note in passing that, if there is an electrostatic attraction between two atom types, then the L-J potential will be more critical than if there is electrostatic repulsion, since the L-J potential form rises steeply in the contact region but is relatively flat (and small) further away. Therefore, when converting L-J parameters for ions from one force field convention to another, it is advisable to match the potential for interaction with an oppositely-charged atom type rather than (in this case) that for cation–cation interactions. These AMBER-adapted parameters are hereafter referred to as the Åqvist/TIP3 parameters. The well depths developed in the Åqvist study ranged from *ca.* 0.02 kcal for Li^+ to 8×10^{-5} kcal for Cs^+ (Table 1). These are orders of magnitude shallower than the one used above (0.1 kcal), yet both parameter sets produced correct relative hydration free energies as well as reasonable hydration free energy for Li^+, as discussed below.

Ion–oxygen radial distribution functions were calculated for the ions in the DNA quadruplex using the Åqvist/TIP3 parameters (Table 1). The internuclear distances at the radial distribution first peaks were slightly larger in DNA than in water for Li^+ and Na^+ but were progressively less than the distances in water as ion size increased to that of K^+ and larger.

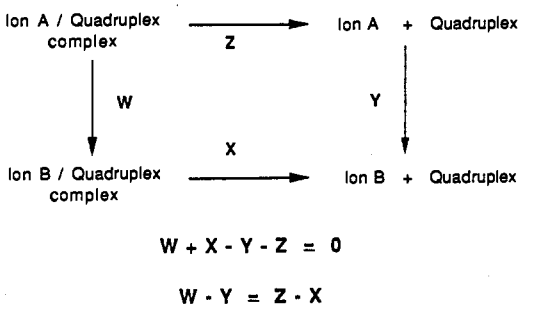

Figure 4. Free energy perturbation cycle. The difference in the free energies of steps W and Y can be determined directly as the difference Z – X, which is determined directly in the free energy perturbation calculations. This corresponds to the differential stabilizing influence of monovalent cations with different radii upon quadruplex formation. Thus, it is not necessary to postulate a mechanism for the more complex reaction steps X and Z.

Parameters arrived at in one environment may not work in another. Marrone and Merz, following the examples of Åqvist, attempted to fit ion L-J parameters to reproduce experimental radial distribution and free energy data for cations in both water *and MeOH*.[53] Other interesting approaches to ion parametrization include calculation of the long-range dispersion (the '12' in the Lennard-Jones 6–12 parametrization) by Kohn–Sham density functional theory (Bartolotti *et al.*[54]) and development of a special force field for ions involving 10–12 and symmetry terms to reproduce crystallographic structures (Vedani and coworkers[55–57]).

Free Energy Perturbations. Size-dependent stabilization of the quadruplex structure by monovalent cations has been attributed to energetically favorable binding of the ion within the octacoordinate cavity formed by the eight O_{GO6} atoms. Formation of the complex depends on the relative energies of the complexed and 'free' (solvated) ions. The free energy differences for binding of different ions ($\Delta\Delta G$s) can be obtained from the thermodynamic cycle shown in Figure 4 by subtracting the free energy differences (ΔGs) due to changing the ion size in water from the corresponding ΔGs calculated for the same range of ions within the complex.[13] While the effects of only one ion were considered in the calculations presented here, more complex interactions involving ions in adjacent binding sites may also contribute to the net stabilizing influence of the ion.[3] Note that the error in free energy due to sampling is at least as large as the hysteresis.

Since this approach does not account for the free energy of quadruplex formation in water, we cannot determine the energy

(36) Kistenmacher, H.; Popkie, H.; Clementi, E. *J. Chem. Phys.* **1973**, *59*, 5842–5848.
(37) Kistenmacher, H.; Popkie, H.; Clementi, E. *J. Chem. Phys.* **1973**, *58*, 1689–1699.
(38) Nguyen, H. L.; Aldeman, S. A. *J. Chem. Phys.* **1984**, *81*, 4564–4573.
(39) Bounds, D. G. *Mol. Phys.* **1985**, *54*, 1335–1355.
(40) Heinzinger, K. *Pure Appl. Chem.* **1985**, *57*, 1031–1042.
(41) Lybrand, T. P.; Kollman, P. A. *J. Chem. Phys.* **1985**, *83*, 2923–2933.
(42) Straatsma, T. P.; Berendsen, H. J. C. *J. Chem. Phys.* **1988**, *89*, 5876–5886.
(43) Chandrasekhar, J.; Spellmeyer, D. C.; Jorgensen, W. L. *J. Am. Chem. Soc.* **1984**, *106*, 903–910.
(44) Berendsen, H. J. C.; Postma, J. P. M.; van Gunsteren, W. F.; Hermans, J. In *Intermolecular Forces*; Pullman, B., Ed.; Kluwer: Boston, 1981; pp 331–342.
(45) King, G.; Warshel, A. *J. Chem. Phys.* **1989**, *91*, 3647–3661.
(46) Bayly, C. Personal communication.
(47) Pauling, L. *The Nature of the Chemical Bond and the Structure of Molecules and Crystals*; Cornell University Press: Ithaca, New York, 1960.
(48) Herdman, G. J.; Neilson, G. W. *J. Mol. Biol.* **1975**, *92*, 181–192.
(49) Neilson, G. W.; Enderby, J. E. *Annu. Rep. Prog. Chem., Sect. C* **1979**, *76*, 195.
(50) Magini, M. In: *Ions and Molecules in Solution*; Tanaka, N., Ohtaki, H., Tamamushi, R., Eds.; Elsevier: New York, 1983; p 97.
(51) Neilson, G. W.; Enderby, E., Jr. *Annu. Rep. Chem.* **1980**, Chapter 7.
(52) Neilson, G. W.; Skipper, N. *Chem. Phys. Lett.* **1985**, *114*, 35–38.
(53) Marrone, T. J.; Merz, K. M. *J. Phys. Chem.* **1993**, *97*, 6524–6529.
(54) Bartolotti, L. J.; Pederson, L. G.; Charifson, P. S. *J. Comput. Chem.* **1991**, *12*, 1125–1128.
(55) Vedani, A.; Dobler, M.; Dunitz, J. D. *J. Comput. Chem.* **1986**, *7*, 701–710.

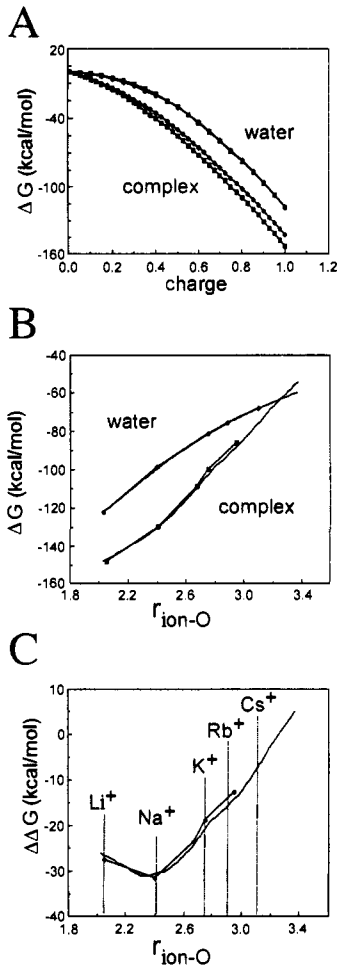

Figure 5. Effect of ionic radius on the quadruplex stabilization free energy. The radii were determined from the formulas described in the legend for Figure 3 and the last column in Table 1. (A) Free energy perturbation results for charging a lithium-sized sphere in water (□, forward; ♦, back) and within the DNA quadruplex (□, forward; ♦, back). (B) Free energies calculated as a function of monovalent cation size in ion–quadruplex and ion–H_2O systems using r^* (–, quadruplex, and H_2O) and both r^* and e (□, quadruplex; ◇, H_2O). (C) Differential free energies for ion-dependent stabilization of the quadruplex as a function of ion radius.

barrier for complex formation; however, we avoid the necessity of defining a specific mechanism for the potentially complicated transition pathway between free and bound states. Note that the bound ion does not interact simultaneously with water and DNA, a situation in which the compatibility of parameters could come into question. For example, such interactions might require the use of separate sets of nonbonded parameters or some optimized hybrid set (including DNA, H_2O, and ions) to account for each type of ion–ligand interaction.

A. Ionic Charge Perturbations. The relative free energies in water and in complex determine ion selectivity: the *absolute* free energies of cation solvation or complexation do not affect the outcome. However, it is interesting to estimate the absolute energy of complexation of the smallest ion, Li^+, in order to compare with the (known) free energy of hydration. We first discuss hydration along with the use of the Born approximation in the context of a distance cutoff of the pairwise electrostatic potential, and then turn to an estimation of the absolute free energy of cation binding in the DNA quadruplex.

The free energy change for charging a neutral sphere was calculated for each environment. This sphere had a L-J well depth of 0.1 kcal, and r^* was set to yield a (charged) ion–oxygen internuclear distance of 1.95 Å (about the size of Li^+). In water, the free energy was –118.5 kcal mol^{-1} (Figure 5A, Table 2). A calculation of the free energy for desolvating the neutral sphere resulted in a nonmonotonic free energy path with a maximum magnitude of less than 1 kcal mol^{-1}. As noted above, the free energy of hydration thus calculated for lithium compares well with experimental values of –118.1[32] and –123.5 kcal mol^{-1}.[31] This agreement is partly due to a cancellation of errors (otherwise known as parametrization), as described in the following paragraph.

The Born model of ion hydration[58] provides a simple correction for artifacts due to use of an ion–water nonbonded cutoff distance[20] (although it does not correct for water–water cutoff). The equation is

$$\Delta G = -\frac{Z^2e^2}{8\pi\epsilon_0 r}\left(1-\frac{1}{\epsilon_r}\right)$$

where Z is the charge of the ion, e is the electronic charge, ϵ_0 is the permittivity of the vacuum, r is the radius of the ion, and ϵ_r is the dielectric constant. Calculating the energy of charging *the sphere of water molecules within the cutoff distance*, rather than a single ion, lessens the sensitivity of the calculations to small differences in the size of cavity that is to be charged.[59] However, periodic systems such as in the present study include the major part of the second order polarization effects, *i.e.* interactions between water molecules within the sphere and those located outside of the sphere.[20] Using our nonbonded ion–oxygen cutoff distance of 8 Å as the size of the Born sphere, the calculated corrections range from –20.3 to –20.4 kcal mol^{-1} for dielectric constants of 50 and 80, respectively. Ignoring second-order effects, this correction results in a free energy of hydration for Li^+ of –140 kcal mol^{-1}, some 20 kcal more negative than the experimentally determined value. Thus, 'errors' in the *van der Waals contributions* to solvation free energy (owing to ion parametrization) may compensate for errors in *charge contributions* owing to use of the cutoff. (This illustrates the nature of the parametrization process.) The experimental energy for solvation of Li^+ chosen by Åqvist (–122.1 kcal mol^{-1} [20]) was used as the basis for our relative free energies of solvation.

To further test the Born approximation under periodic boundary conditions, the free energy of charging the Åqvist/TIP3 Li^+ ion was calculated in a 37-Å box containing 1726 waters, using progressively larger cutoff distances of 4, 8, and 12 Å. The Born approximation *over*compensates by *ca.* 11 kcal mol^{-1} in each case, *e.g.* the 'correction' is more than double the amount required for the 8-Å cutoff (Table 3). Therefore the Born correction should be used with caution in systems that allow second-order interactions between molecules in the ion cutoff sphere and those outside. The densities for the perturbations with the three cutoffs were 0.93, 0.98, and 1.0 g cc^{-1}, respectively. However, a second perturbation with the 4-Å cutoff using constant volume to achieve the proper density gave the same result (–93 kcal mol^{-1} compared to –90 kcal mol^{-1} for the constant pressure perturbation).

The free energy for charging the lithium-sized sphere within the DNA quadruplex was –148.5 kcal mol^{-1} (Figure 5A, Table 2B). In this case, *all* of the ion–DNA interactions were calculated, including those of the counterions in solution, so the effective Born sphere for the central ion is larger than that for a single ion in water and is not properly spherical as required by the Born approximation. Values for the Born correction range from –16 to –10 kcal mol^{-1} for radii of 10 and 15 Å, respectively, approximately equal to the error in the Born correction encountered with water, above. The non-'corrected' –148.5 kcal mol^{-1} value was used as the basis for our radial perturbations in the quadruplex using both sets of ionic nonbonded parameters.

The simulation times used to charge the spheres were 12.5 ps for water and 25 ps for the complex. The Born charging comparisons in water used 0.5–0.75 ns each. For the radial

(56) Vedani, A.; Huhta, D. W.; Jacober, S. P. *J. Am. Chem. Soc.* **1989**, *111*, 4075–4081.
(57) Vedani, A.; Huhta, D. W. *J. Am. Chem. Soc.* **1990**, *112*, 4759–4767.

Table 2. Effect of Ion Charge on Ion Free Energy in H_2O and within the DNA quadruplex

charge range	no. of windows (run type)	no. of H_2O	free energies (kcal mol^{-1}) fwd path fwd	fwd path rev	rev path fwd	rev path rev	sum (fwd)	mean (|fwd|)	% hysteresis
			A.In H_2O						
1.0									
	21[a]	876	119.0	−119.0	−118.1	119.0	0.9	118.5	0.8
0.0									
			B.In Quadruplex						
1.0									
	21[b]	2413	159.7	−157.4	−145.6	148.4	14.1	152.6	9.2
	41[b]	2413	153.6	−153.0	−143.4	144.5	10.2	148.5	6.5
0.0									

[a] 200 steps of equilibration plus 400 steps of sampling (total time of 1.2 ps) per window. [b] 400 steps of equilibration plus 400 steps of sampling (total time of 1.6 ps) per window.

Table 3. Test of the Born Charge Approximation in H_2O under Periodic Boundary Conditions

cutoff (Å)	free energy[a] (kcal mol^{-1})	% hysteresis	deviatn from target[b] (kcal mol^{-1})	born correctn (kcal mol^{-1})	simulatn time (ns)	CPU cost factor[c]
4	−90.54	0.2	−32	−41	1.1	1.0
8	−114.03	0.4	−8	−21	1.5	2.4
12	−117.95	0.4	−4	−14	1.4	5.9

[a] Free energy of charging a neutral sphere having Åqvist/TIP3 Li^+ L-J parameters in water using AMBER 4.1. [b] Target chosen by Åqvist for Li^+ (122.1 kcal mol^{-1}). Other experimental values: −118.1[32] and −123.5 kcal mol^{-1}.[31] [c] CPU cost as a factor of the time expended on the 4-Å calculation (93 h on a Convex 3800).

perturbations using fixed well depths, the total times used to convert Li^+ to Cs^+ were 97.2 ps in water and 232 ps in the complex, where twice as much time per window (0.2 ps) was used to equilibrate the system for most runs. For the *radial* perturbations in the complex with the Åqvist/TIP3 ion parameters, the total simulation time was 656 ps. An equal amount of simulation time was used for the forward and reverse pathways in each case (see Table 2). A single perturbation was also performed by transforming the Åqvist/TIP3 Na^+ into K^+ within the Kang *et al.*[28] structure using the 'dynamic windows' feature introduced in AMBER 4.0.[18] This perturbation required 128 ps and duplicated the result obtained with AMBER 3.0 Revision A[17] for the Williamson *et. al.* structure (Table 4C).

The free energies for charging Li^+ described above (Figure 5A) were used to position the radial perturbation curves on the free energy axis (Figure 5B). These curves were then subtracted to yield the radius-dependent differential free energies of solvation for monovalent cations (Figure 5C). Note that this difference curve can only be meaningful if the ion–oxygen internuclear distances are the same within the complex as in solution; this assumption is examined below. First, we describe the radial perturbations in each environment in detail.

B. Ionic Radial Perturbations in Water. A single ion was perturbed from the radius of Li^+ to that of Cs^+ in water for comparison with the same perturbation of a single ion within the quadruplex binding cavity. While the single ion in the quadruplex has a highly structured environment, an ion in solution is subjected to a wider range of environments which might affect the perturbation differently. To determine whether other types of ion solution environments could produce different hydration free energies (ΔG_{hyd}), a cation was perturbed in water in the presence of other solutes. In these perturbations, the ion r^* value was decreased from 1.7 to 0.7 Å (with a constant well depth of 0.1 kcal) in 20 windows, each consisting of 200 equilibration steps and 400 data gathering steps. In the lone ion case, the initial water boxes extended axially 10.5 Å from the ion–solute centers, giving a total of 253 water molecules.

In one test, we perturbed a pair of cations bound to oxygens from two water molecules (a configuration we have observed in this and other studies) to see if this geometry significantly affects the free energy. In another test, a single cation was perturbed near a backbone phosphate in a DNA trinucleotide duplex, with three unperturbed cations similarly placed near the other phosphates, to see how the anionic phosphodiester environment affected the relative ΔG_{hyd}. The free energies were −56 and −55 kcal mol^{-1} of cations, respectively, virtually identical to the value obtained with a lone cation in water, −56 kcal mol^{-1}. The free energy for size-perturbing a single ion in the bath of 253 waters exhibited a 4 kcal mol^{-1} hysteresis (7%) in the reverse pathway. The lone ion calculation was repeated using a 9-Å cutoff distance (−55 kcal mol^{-1}, 8% hysteresis) and an 8-Å cutoff with a larger box (31-Å sides vs. 21 Å) containing 876 water molecules (−56 kcal mol^{-1}, 4% hysteresis). The cation–O and O–O radial distributions for 8-Å and 9-Å cutoff distances (r^* = 1.7 Å) were superimposed, and the effect of varying the cutoff distance was found to be insignificant. The larger system was used for comparison of free energies with values obtained with the complex. The time used to convert Li^+ to Cs^+ and back in H_2O with a fixed well depth was 97.2 ps in each direction. The free energy curve superimposes with that of Åqvist[20] (Figure 5B), which in turn matches the experimental data.

C. Ionic Radial Perturbations within the Quadruplex. The four-stranded G-DNA model of Williamson *et al.* was used for cation size perturbations in the complex. The system consisted of 524 DNA atoms, the internally bound cation, 12 "Na^+" counterions and water. In one case, 2413 water molecules were used, totaling 7776 atoms; in another 1704 waters were used, totaling 5649 atoms. For the fixed well depth calculations, the perturbation was divided into multiple segments such that the radius increment per window was decreased as the change in energy increased—a crude approximation of the 'dynamic windows' method[18] (Table 4B). The curves for the segments were each averaged across forward and reverse paths, adjoined to form a single overall curve, and then the X-axis was converted from r^* units to units of ion–oxygen internuclear distance. When hysteresis became a problem, the increment parameter $\Delta\lambda$ was decreased to allow more careful sampling and/or the smaller system was used to allow more rapid equilibration. A Na^+ ⟨-⟩ K^+ perturbation was also performed in the Kang *et al.* structure using 2831 waters (total of 9030 atoms).

In the fixed well depth perturbations, as the ion–oxygen internuclear distance reached and exceeded that of K^+ in water (r^* > 2.0 Å, r(ion–GO6) > 2.79 Å), hysteresis proved insurmountable. A longer run (130 ps) with the smaller box varying

Table 4. Effect on Ion Radius on the Free Energy in H_2O and within the DNA Quadruplex

			free energies (kcal mol^{-1})						
			fwd path		rev path				
r (Å)	no. of windows (run type)	no. of H_2O	fwd	rev	fwd	rev	sum (fwd)	mean (|fwd|)	% hysteresis
			A.In H_2O						
0.7									
	81[a]	876	82.8	−82.3	−80.8	81.5	2.0	81.8	2.4
2.5									
			B.In Quadruplex						
0.7									
	21[b]	2413	22.3	−21.3	−22.8	23.5	−0.5	22.5	2.2
1.4									
	21[b]	2413	32.2	−31.3	−30.8	31.0	1.4	31.5	4.4
2.0									
	21[b]	2413	9.0	−9.0	−9.1	9.6	−0.1	9.1	1.1
2.2									
	21[b]	2413	10.8	−10.7	−8.9	8.9	1.9	9.9	19.3
2.4									
	21[b]	2413	12.1	−11.9	−10.3	10.4	1.8	11.2	16.1
2.6									
	21[a]	2413	10.1	−9.9	−9.4	9.4	0.7	9.8	7.2
2.8									
	21[a]	2413	10.0	−9.9	−9.7	9.7	0.3	9.8	3.0
3.0									
	21[a]	2413	8.3	−8.1	−6.5	6.6	1.8	7.4	24.3
3.2									
2.0									
	81[b]	1704	31.7	−32.2	−22.1	22.5	9.6	26.9	35.7
2.6									
			C.In Quadruplex (Åqvist/TIP Ion Parameters)						
'Li$^+$'									
	41[b]	2413	18.0	−17.9	−19.5	20.1	1.5	18.8	8.0
'Na'									
	41[b]	2413	22.4	−22.3	−17.8	17.8	4.6	20.1	22.9
	41[b]	1704	21.5	−21.5	−20.8	20.8	0.7	21.1	3.3
	107[c]	2831			−20.0				
'K$^+$'									
	41[b]	2413	7.4	−7.4	−9.2	9.2	−1.8	8.3	21.7
	41[b]	1704	8.8	−8.8	−8.9	8.9	−0.1	8.8	1.1
'Rb$^+$'									
	41[b]	2413	15.5	−15.4	−12.3	12.3	3.2	13.9	23.0
'Cs$^+$'									

[a] 200 steps of equilibration plus 400 steps of sampling (total time of 1.2 ps) per window. [b] 400 steps of equilibration plus 400 steps of sampling (total time of 1.6 ps) per window. [c] 'Dynamic windows' with Kang *et al.* model: 200 steps of equilibration plus 400 steps of sampling per window.

r^* from 2.0 to 2.6 Å and back (total 260 ps) failed to converge. A 30% hysteresis was obtained due to *disruption* of the quadruplex by the *larger ions*. Hydrogen-bonding and stacking interactions were severely disrupted. A root mean square fit of the central eight bases to the starting structure increased from 0.4 Å at r^* = 2.15 Å to 1.4 Å at r^* = 2.6 Å and was 1.3 Å at the end of the return path. The r^* = 2.0–2.6 Å perturbation with the smaller box yielded approximately the same free energy as the shorter perturbation with the larger box, and the data from the larger box were used to construct the curve for the fixed well depth perturbation (Figure 5B).

The initial perturbations with the Åqvist/TIP3 parameters used the larger system. Increased hysteresis (*ca.* 20%) was also seen as the ion reached the size of K^+, so the Na^+ ⟨-⟩ K^+ and K^+ ⟨-⟩ Rb^+ perturbations were redone using the smaller box and the same amount of simulation time. This produced converged free energies (4% and 1% hysteresis, respectively) within 1 kcal mol^{-1} of the mean values obtained in the initial paths. The ion-O_{GO6} internuclear distances assigned to the Åqvist/TIP3 ion free energies in Figure 5B are the first peaks of our calculated radial distribution functions (Table 1, rightmost column). Linear interpolation was performed between each point to derive energies at ion-O_{H_2O} internuclear distances. The free energies of the ions in water were subtracted from these energies to obtain ion size-dependent $\Delta\Delta G$ values for the Åqvist/TIP3 ions. The size-dependent free energy curves for the simple and Åqvist/TIP3 ion parameters in the complex are very similar (Figure 5B and C).

While similar free energies for 'growing' and 'shrinking' the ion were obtained with both sets of parameters, the structural consequences of growing the ion beyond the apparent size of the DNA cavity seemed to be more pronounced when the 0.1 kcal well depth was used. As the cavity expanded, O6 atoms on the terminal bases would often bind to the ion in the central binding cavity. A striking case is shown in Figure 6A, where the interaction between the terminal base and the ion help to preserve the labile stacking interactions between neighboring bases on the same strand. In another, more unique case of structural disorder, a terminal base moved out of its plane, dissociated from a G-quartet leaving a terminal G-triplex (Figure 6B), and moved into the adjacent plane, where it formed a bifurcated hydrogen bond with the adjacent base on its own strand (Figure 6C).

D. Comparative Free Energies for Ion Perturbations in Water and within the Quadruplex. Increasing the cation radius produced a progressively smaller increase in ΔG in water and a progressively larger increase in ΔG within the quadruplex with both sets of ion L-J parameters (Figure 5B). We attribute the former result to the easier deformability of water as the ionic charge density diminishes (*i.e.* 'size' increases), consistent with results from the charge perturbation with a fixed ion radius (Figure 5A). We attribute the latter result to the relative rigidity of the ion-binding site within the quadruplex. Base–base hydrogen bonds, stacking interactions, and perhaps constraints imposed by the phosphodiester backbone and the surrounding water structure presumably set an upper limit on the energetically feasible range of cation

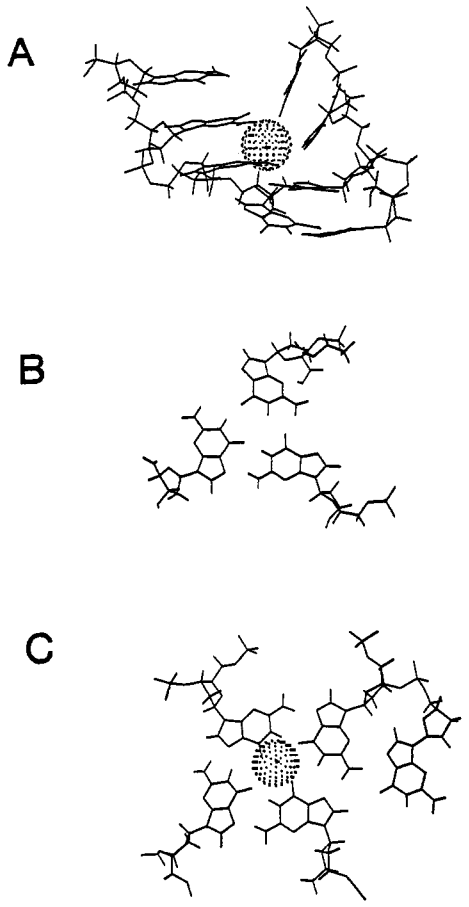

Figure 6. Three examples of structural changes observed during molecular dynamics with the antiparallel DNA quadruplex containing a single internally bound cation at an ion–O_{GO6} radius of >2.8 Å (larger than K^+). (A) Cutaway view from the center of the complex showing the GO6 of the terminal base on the upper right "collapsed downward" to bind to the cation instead of the terminal base on the upper left. (B) Terminal triplex. (C) Adjacent five-stranded structure formed as a result of a disproportionation reaction during molecular dynamics.

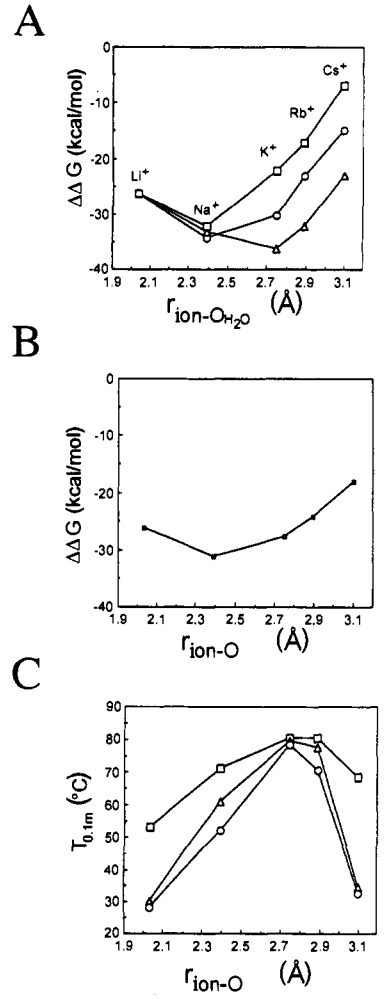

Figure 7. (A) Hypothetical free energy difference curves calculated assuming ion–oxygen internuclear distances are smaller in the complex than in H_2O. Same distances in the complex and in water (■), from Figure 5C; distances in complex reduced by 0.2 Å (●); distances in complex reduced by 0.4 Å (▲). (B) Free energy difference curves resulting from the assumption that Åqvist/TIP3 ion parameters are correct in DNA; *i.e.*, only K^+, Rb^+, and Cs^+ ions are smaller in complex than in water. (C) Experimental thermal denaturation temperatures plotted as a function of cation-oxygen internuclear distance for parallel-stranded quadruplexes formed by d(CGC G_3 GCG) (▲),[3] d(m^5C G m^5C G_3 G m^5C G) (■),[50] and d(TAT G_4 ATA) (●).[50]

radii. Beyond this size, steric repulsion energies increase, and eventually the stacking and hydrogen-bonding interactions are disrupted. The GO6 'ligands' do not interact with the smaller ions as effectively because the cavity cannot shrink to maintain the same optimized octahedral contacts.

The relative 'preference' of different ions for the complex over water is shown by the free energy difference ($\Delta\Delta G$) curves (Figure 5C). The Na^+ ion is favored by 5 kcal mol^{-1} over Li^+ and by 13 kcal mol^{-1} over K^+. The preference of Na^+ over Li^+ supports the notion that the ion must fit the cavity properly for stabilization of the quadruplex to occur. However, the preference of Na^+ over K^+ does not agree with experimental melting temperature (T_m) results which demonstrated that quadruplexes constructed from short G-rich oligonucleotides [3] (Figure 7C) or guanosine-5′-monophosphate gels[8] are more stable in K^+ than in Na^+ (T_m values differ by *ca.* 17 °C). Four possible explanations are as follows: (1) The oxygen–cation internuclear distance may be smaller within the complex than in water. (2) The quadruplex binding cavity may be too small (as a result of an incorrect structural model or artifacts due to the force field). (3) Sampling of ion positions in the binding cavity may be inadequate. (4) Finally, the form of the force field, involving pairwise calculation of the electrostatic potential, may be inadequate for such situations, which might involve polarization and/or electron delocalization effects. We now proceed to examine each explanation in turn.

E. Ion Parameter Adjustments. To determine how much smaller the ion–oxygen internuclear distances would have to be to match the melting temperature data, the ion sizes in the complex were assumed to be 0.2 and 0.4 Å smaller than those in H_2O, and the resulting free energy curves were subtracted from that obtained in H_2O (Figure 7A). The experimentally observed preferential stabilization of the quadruplex by K^+ (Figure 7C) is reproduced when the 0.4 Å smaller ion–oxygen radii are assumed, yielding a preferred stabilization by K^+ relative to Na^+ of 4–5 kcal mol^{-1}. This value for the per-ion $\Delta\Delta G$ is reasonable considering the relatively large differences in T_m values obtained experimentally with [d(PuPyPu G_n PyPuPy)$_4$– cation$_m$] complexes[3,60] (Figure 7C). Experimental ΔG values are not presently available due to difficulties in making comparative equilibrium thermodynamic measurements under strictly reversible conditions.

Instead of an arbitrary uniform reduction in ion–GO6 internuclear distances, one can use the internuclear distances resulting from the use of the Åqvist/TIP3 ions in the complex (Tables 1 and 5). This approach is more reasonable because the sizes of the smaller ions are preserved. The resulting $\Delta\Delta G$ (complex–water, K^+–Na^+) still favors Na^+ over K^+, although the difference is reduced from 13 to 3.5 kcal mol^{-1} (Figure 7B, Table 5). The

(58) Born, M. *Z. Phys.* **1920**, *1*, 45.

Table 5. Effects of Alternative Ion Lennard-Jones Parameters on Na^+/K^+ Selectivity

	e (kcal)		r^* (Å)		$R_{ion-GO6}$		$\Delta\Delta G$
	Na^+	K^+	Na^+	K^+	Na^+	K^+	(kcal mol^{-1})
ion–GO6 = water	0.1	0.1	1.39	1.93	2.39	2.75	13
ion–GO6 < water	0.1	0.1	1.38	1.79	2.39	2.66	1.4
Åqvist/DNA	0.0028	0.000 33	1.86	2.63	2.33	2.61	2.7
Åqvist/TIP3	0.0028	0.000 33	1.87	2.66	2.40	2.67	3.5
Åqvist(pot_{dna} = water)	0.0028	0.000 33	2.04	2.83	2.47	2.72	5.5
Marrone & Merz[a]	0.040	0.035	1.70	2.17	2.49	2.72	7.8

[a] See ref 53.

same result was also obtained with the crystallographic structure of Kang *et al.* (Table 4C). Another alternative is to derive seperate r^* parameters for the Åqvist ions in the complex, as was done with water, such that the ion–GO6 minimum-energy point is the same as with the 6–12 combining rules used by Åqvist (referred to as Åqvist/DNA ion parameters). This yields smaller ion–GO6 internuclear distances and a slightly better $\Delta\Delta G$ (favoring Na^+ *less* over K^+) of 2.7 kcal mol^{-1} (Table 5). We also tried setting the Åqvist ion r^* in the complex so that the ion–GO6 potential minimum was at the same distance as the Åqvist/TIP3 minimum, but this yielded larger ions and a less satisfactory $\Delta\Delta G$ of 5.5 kcal mol^{-1} (Table 5). The parameters derived for water and MeOH by Marrone and Merz[53] yielded the largest ions of all and a less satisfactory $\Delta\Delta G$ (favoring Na^+ *more* over K^+) of 7.8 kcal mol^{-1} (Table 5).

Finally, it turns out that the best $\Delta\Delta G$ (but still not proper ion selectivity), 1.4 kcal mol^{-1}, is obtained if one uses the fixed well depth of 0.1 kcal mol^{-1} and assumes that the r^* parameters for the ions in water are 'correct' for the complex (Figure 7C, Table 5). This assumption implies ion–GO6 distances of 2.39 and 2.66 Å for Na^+ and K^+, respectively. These are uniformly 0.01 Å less than the internuclear distances obtained with the Åqvist/TIP3 ions (but with a $\Delta\Delta G$ 2.1 kcal mol^{-1} closer to Na^+/K^+ equality) and are larger than those obtained with the Åqvist/DNA ions. Thus, although the radial free energy curves for the ion in the complex in Figure 5B align well, the combination of L-J parameters used to obtain a given size may make a critical difference in the free energy. The 'softer' $e = 0.1$ may compensate for an electrostatic (many-body) effect not modeled by the force field. The Na^+/GO6 distance is within the experimental range for water, but the K^+/GO6 distance is 0.14 Å smaller than the smallest experimental value (Table 1; note that the 'target' size for K^+ adopted from Åqvist is closer to the sum of the Pauling radii than to experimental results).

F. DNA Cavity Size. An ion-binding cavity that is too small would be an alternative steric explanation for the selection of Na^+ over K^+. The cavity size in the Kang *et al.* structure was further examined by holding the DNA fixed and energy minimizing an oversized ($r^* = 4.9$ Å) neutral probe atom in the cavity. The closest probe–GO6 interatomic distance was 2.46 Å. The average probe–GO6 distance was 2.66 Å, omitting a single, clearly noncontacting distance of 4.78 Å. This is comparable to the radial distribution first peak of 2.67 Å obtained in the Williamson *et al.* structure at 300 K with the Åqvist/TIP3 K^+ ion. An oversized probe atom was also placed in the cavity of the Kang *et al.* structure that had been equilibrated without a bound ion in water and then averaged over an interval and energy minimized. The average probe–GO6 distance was 2.72 Å, omitting two distances greater than 3 Å. The average probe–GO6 distance was 2.84 Å in the Williamson *et al.* structure, omitting one distance greater than 3 Å. When each of these two structures was energy minimized with an Åqvist/TIP3 Na^+ ion to a root mean square gradient of 0.001, the average probe distances were almost identical: 2.49 Å for Williamson *et al.* and 2.48 Å for Kang *et al.* Since the unoccupied cavity of the Williamson structure is larger than our target ion–oxygen distance for K^+ (probe of 2.84 vs 2.75 Å for K^+) and resembles ion–oxygen distances found in crystals of the [K^+–(C222)–e^-] electride complex (2.80–2.86 Å),[61] we believe that the preference for Na^+ over K^+ does not stem from too small a cavity.

G. Sampling of the DNA Cavity. When the bound ion is not large enough to be coordinated with all eight DNA oxygens, it is possible that sampling is insufficient because the positions in the cavity may not all be reached during the time span of the trajectory. Note that in this case, the mass term would *not* drop out of the free energy equation because at each window of the perturbation the average velocity of the ion relative to its environment would not be 0; *i.e.*, sampling would be insufficient to capture the entire time–correlation function, the requirement for strict convergence to an equilibrium in the calculation. The narrow shape of the ion–oxygen radial distribution for $r^* = 1.5$ Å in Figure 3A suggests that neither incomplete coordination nor the associated possibility of inadequate sampling affect Na^+/K^+ selectivity, because even the smaller versions of the Na^+ ion were uniformly coordinated within the octahedral site. Nonetheless, in order to improve the sampling and test the theoretical independence of free energy from mass variations, we compared free energies for perturbing Na^+ ⟨--⟩ K^+ in the complex using the (smaller) Åqvist/DNA parameters and using fixed ion masses of 0.5, 6.94 (Li^+), and 22.99 au (Na^+). The results were essentially the same: 20.6 kcal mol^{-1} with 3% hysteresis; 20.3 kcal mol^{-1} with 2% hysteresis; and 20.0 kcal mol^{-1} with 15% hysteresis, respectively. The markedly lower hysteresis with the two less massive ions confirms the rationale for using smaller masses for perturbed particles (we believe that the slightly larger hysteresis with the mass of 0.5 au is a result of the 2-fs time step, which is too long to capture the higher frequency motions of such a light particle). Note that the issues discussed in this paragraph do not address conformational sampling of the DNA itself; however, the similarity of the free energy results for the two different DNA structures implies that this too is not an issue.

H. Force Field Considerations. Strahan and co-workers have recently found that K^+ seems to weaken the G–G hydrogen-bonding network in the bimolecular $d(G_3T_4G_3)_2$ complex, where the 'outer', N7-amino hydrogen bonds (N7···HN2–N2) are particularly affected (NMR results).[62] We believe that less connectivity at the periphery may indicate that K^+ is large enough to disrupt the canonical quadruplex structure, which implies that the K^+/O internuclear distance is the same whether the oxygen atom is a constituent of H_2O or the aromatic guanine base. Thus, in the size-consistent free energy curves, K^+ is located at or near a shoulder which may represent the breaking of the amino hydrogen bonds (Figure 5A, B at $r_{ion-O} = 2.8$ Å). Hydrogen-bonding distances for dynamics with the Kang *et al.* structure with Na^+ and K^+ are shown in Table 6. The N7-amino hydrogen bond is marginally weakened by K^+ (by 0.03 Å), but the inner O6–N1 hydrogen bond is strengthened somewhat more (by 0.09 Å). Note that the deviation in ion–O6 distance is significantly greater for Na^+ (0.2 Å as opposed to 0.1 Å for K^+).

If the $d(G_3T_4G_3)_2$ results pertain to our calculations with $d(G_4)_4$, we can infer that the wrong preference for Na^+ over K^+ in our case stems from inadequate treatment of electronic effects involved in stacking or $K^+/(O6)_8$ coordination. The weakened N7-amino hydrogen bonding in the grooves must be compensated for in some way, perhaps by subtle improvements in stacking energies via conformation or by electron density redistribution from the partially anionic N7 in the imidazole ring to the six-membered ring via the polarizable π system, either enhancing aromatic π–ion interactions or strengthening the ligand–cation bond character. Thus, in addition to the size difference between Na^+ and K^+, these ions may differ in their abilities to form cation–GO6 salt bridges or to support electron delocalization. The valence orbitals

(59) Rashin, A. A.; Honig, B. *J. Phys. Chem.* **1990**, *46*, 165–179.
(60) Hardin, C. C.; Corregan, M. J.; Brown, B. A., II; Frederick, L. *Biochemistry* **1993**, *32*, 5870–5880.

Table 6. G·G Hydrogen Bond Distances in the Na^+ and K^+ Quadruplexes[a]

interaction	Na^+ complex (Å)	K^+ complex (Å)
cation–O6[b]	2.50 (±0.23) (range = 2.09, 3.97)	2.78 (±0.13) (range = 2.45, 3.81)
	Central 2 G-Quartets[b]	
N2–N7	2.89 (±0.13) (range = 2.56, 3.78)	2.92 (±0.14) (range = 2.57, 3.91)
N1–O6	3.03 (±0.19) (range = 2.61, 4.05)	2.94 (±0.16) (range = 2.58, 3.90)
	Outer 2 G-Quartets[c]	
N2–N7	3.21 (±0.78) (range = 2.54, 6.28)	3.15 (±0.50) (range = 2.71, 5.20)
N1–O6	3.11 (±0.43) (range = 2.52, 4.81)	3.07 (±0.36) (range = 2.62, 4.14)

[a] DNA Kang *et al.*; ion well depth of 0.1 kcal mol^{-1}; r^* = 1.39 Å (Na^+) and r^* = 1.93 Å (K^+). [b] Averaged over 60 ps. [c] Na^+ averaged over 30 ps; K^+ averaged over 20 ps.

of potassium are more diffuse than those of sodium, as indicated by $M \rightarrow M^+$ ionization energies (potassium, 100 kcal mol^{-1} < sodium, 118 kcal mol^{-1}) and $M \rightarrow M^-$ electron affinities (potassium, 11 kcal mol^{-1} < sodium, 13 kcal mol^{-1}).[63] Moreover, the K^+ (cryptand [2.2.2]) complex (but not other group I cations) forms an electride salt, in which stoichiometric amounts of trapped or itinerant electrons serve as anions, indicating that the electrons can either be delocalized or are located in shallow traps.[61] It is also interesting to note that the stoichiometric ratio of K^+ to buckminsterfullerene (C60) can dramatically affect electron delocalization between cation-linked C60 ligands, producing complexes that range from superconductive to semiconductive and even nonconductive.[64-66]

Weakening or loss of N7-amino hydrogen bonding would also affect the hydration pattern in the vicinity of the grooves, involving solute size-dependent electrostriction contributions to the free energy which may be sensitive to any incompatibility of the AMBER and TIP3 force fields.[67-72] We must also remember that the results might differ if cations were bound in adjacent sites in the quadruplex. However, in view of the difficulty (using the force field as described) of keeping ions in the adjacent sites simultaneously with the central one and because of the evidence for weakening of the amino hydrogen bonds by K^+, as well as the evidence for K^+-related electronic effects in other systems presented above, it seems possible that Na^+/K^+ selectivity is electronically determined and thus would require additional force field terms such as polarization to model effectively. The full coordination of Na^+ *as well as* K^+ suggests that subtle electronic effects may determine Na^+/K^+ selectivity, while steric disruption determines K^+/Rb^+ selectivity.

Conclusions

Free energy perturbation studies show directly that different group IA monovalent cations should differentially stabilize DNA quadruplexes by partitioning to different extents between the central ion-binding cavity and 'bulk' H_2O. Intermediate-sized ions in the series preferentially stabilize the quadruplex in the calculations, as in experimental studies. In general, smaller ions 'shrink the cage' and larger ions raise the free energy by 'outgrowing the cage' and increasing unfavorable strain energies. However, this does not explain Na^+/K^+ selectivity, which we believe may be due to electronic effects not captured by the electrostatic model, since some compensation must exist for the observed weakening or breaking of the 'outer', N7-amino hydrogen bonds in the K^+ complex compared to the Na^+ one. Perhaps the size difference of the ions affects stacking interactions, or possibly the difference is due to the different electronic nature of the two ions—we infer that K^+ may increase electron delocalization in the guanine aromatic π system and enhance the 'inner' hydrogen bonding and/or the octacoordinate ion–oxygen interactions. Thus, polarization terms or other modifications to the form of the force field may be needed to properly reproduce Na^+/K^+ selectivity.

If K^+ does induce extra electronic delocalization and if K^+ ions exist in adjacent sites, in addition to having possible structural roles in K^+-switched gene regulation,[3-7] G-quadruplexes may function as electronic 'nanowires'. The conductive properties of these structures are presently under investigation.

This system thus lends itself to investigation of polarization effects in macromolecules and to efforts to develop consistent ion force field parameters for interactions with water and macromolecules, especially if experimental free energies can be obtained for the complex. A further question is whether the combination of TIP3 water and AMBER DNA force fields can also be improved, perhaps in conjunction with developing better ion parameters. Subtle changes in the model used to describe the surrounding water can affect macromolecular conformation (and energies), even in the absence of strong (*i.e.* fully 'ionic') charge interactions. For example, different stacking configurations were adopted by both d(AAA) and d(TTT) during dynamics when TIP3 water was used, as opposed to a nonspherical water model with TIP3 charges, individual oxygen and hydrogen r^* values of 1.65 and 1.0 Å, respectively, and no hydrogen–hydrogen SHAKE distance constraints.[73] An alternative to using a unified force field would be to develop special sets of parameters for water–solute (as opposed to water–water) interactions and perhaps ion–solute interactions. The use of multiple parameter sets is common in studies with smaller systems but has seen less application with macromolecular calculations. The GROMOS force field uses a per-pair L-J potential rather than a per-atom one to avoid the limitations of simple combination rules.[22] Simulations using mixed self-consistent force fields are now common (in this case a hydrated macromolecule), so such issues may bear investigation.

Acknowledgment. We wish to thank Gary Strahan for sharing NMR results, Peter Kollman for encouragement and suggestions, Christopher Bayly for sharing results of experiments with the Åqvist/TIP3 ion parameters, Andrew Pohorille for discussions concerning ion parametrization, Uli Schmitz for discussions of ion–DNA interactions, and Andrew Riell for help in figure preparation. This work was supported in part by NIH Grant GM47431 and the North Carolina Agriculture Research Service. Computer resources were generously provided by the North Carolina Supercomputing Center; molecular graphics images were produced using the Midas Plus program by the Computer Graphics Laboratory at UCSF (supported by NIH Grant No. RR-01081).

(61) Huang, R. H.; Faber, M. K.; Moeggenborg, K. J.; Ward, D. L.; Dye, J. L. *Nature* **1988**, *331*, 599–601.
(62) Strahan, G. Personal communication.
(63) Emsley, J. *The Elements*; Clarendon Press: Oxford, U.K., 1989.
(64) Curl, R. F.; Smalley, R. E. *Sci. Am.* **1991**, October, 54–62.
(65) Rosseinsky, M. J.; Murphy, D. W.; Fleming, R. M.; Tycko, R.; Ramirez, A. P.; Siegrist, T.; Dabbagh, G.; Barrett, S. E. *Nature* **1992**, *356*, 416–603.
(66) Chen, C. T.; Tjeng, L. H.; Rudolf, P.; Meigs, G.; Rowe, J. E.; Chen, J.; McCauley, J. P., Jr.; Smith, A. B. III; McGhie, A. R.; Romanow, W. J.; Plummer, E. W. *Nature* **1992**, *356*, 603–605.
(67) Rentzeperis, D.; Kupke, D. W.; Marky, L. A. *Biophys. J.* **1994**, *66*, A25.
(68) Colombo, M. F.; Rau, D. C.; Parsegian, V. A. *Science* **1992**, *256*, 655–659.
(69) Sharp, K.; Nicholls, A.; Fine, R.; Ni, X.; Honig, B. *Biophys. J.* **1991**, *59*, A221.
(70) Hanlon, S.; Pack, G. *Biophys. J.* **1994**, *66*, A154.
(71) Li, Z. Q.; Giege, R.; Jacrot, B.; Oberthur, R.; Thierry, J.-C.; Zaccai, G. *Biochemistry* **1983**, *22*, 4380–4388A.
(72) Dill, K. A. *Biochemistry* **1990**, *29*, 7133–7155.
(73) Ross, W. S., Unpublished results.